Consequences of thermo-oxidative ageing on the microstructure and mechanical properties of blends of polyethylenes with different butene contents

Geraldine Rapp, Jonathan Tireau, Pierre-Olivier Bussiere, J.-M. Chenal, Jean-Luc Gardette, Sandrine Therias, Laurent Chazeau

Consequences of thermo-oxidative ageing on the microstructure and mechanical properties of blends of polyethylenes with different butene contents

Geraldine Rapp[1], Jonathan Tireau[3], Pierre-Olivier Bussiere[1], Jean-Marc Chenal[2], Jean-Luc Gardette[1], Sandrine Therias*[1], Laurent Chazeau*[2]

1 Université Clermont Auvergne, CNRS, Clermont Auvergne INP, ICCF, F-63000 Clermont-Ferrand, France
2 Université de Lyon, INSA Lyon, MATEIS, UMR CNRS 5510, 7 avenue Jean Capelle, F-69621 Villeurbanne, France
3 EDF R&D, Materials and Mechanics of Components Department, Chemistry and Materials for energy efficiency Group, Avenue des Renardières, F-77818 Moret-sur-Loing, France

Abstract

The microstructure of crosslinked blends of PE (containing 3.4 wt. % of butene comonomer) with PEcB (containing 9.4 wt.% of butene comonomer) can roughly be deduced from the microstructure of each PE (indicating a kind of phase separation process at the scale of crystallites), even though there is an important fraction of cocrystals made of chains of both PEs. Their thermo-oxidative ageing mainly leads to chain scissions. Annealing and chemi-crystallization occur in relation to the fraction of both homopolymers. The crystallised chains are protected from chain scission, and their presence at the ageing temperature has direct consequences on the way the elastomer network, initially created by the process, is modified. Thus, when the ageing temperature does not melt the large crystallites, these crystallites protect the long chain portions between chemical crosslinks. In addition, the larger the PE quantity is, the more the crystallites gather to form large scale structure, thereby promoting the percolation of the amorphous cut chains out of this structure. The mechanical behaviour of the materials at ambient temperature or at temperatures above their melting temperature, is the result of all these mechanisms. Thus, the crosslinked blend of 50wt%. of PE and 50wt.% of PEcB may be the best compromise in terms of mechanical properties and their preservation during thermo-oxidation.

Keywords *branched polyethylene; elastomer; blends; thermo-oxidation; microstructure; morphology; mechanical properties*

* Corresponding Author:
Laurent Chazeau
MATEIS UMR 5510 – INSA Lyon
Université de Lyon – CNRS – INSA Lyon
7 avenue Jean Capelle
69621 Villeurbanne Cedex
E-mail: laurent.chazeau@insa-lyon.fr

Sandrine Therias
I.C.C.F. UMR 6296 - Institut de Chimie de Clermont-Ferrand
Université Clermont Auvergne - CNRS - SIGMA Clermont
Campus des Cézeaux - 24, avenue Blaise Pascal - TSA 60026 - CS 60026
63178 Aubière Cedex
E-mail: sandrine.therias@uca.fr

1. Introduction

In some of their applications, polymer materials must be designed to withstand elevated temperatures. Even when temperatures are not extreme, for instance, below 70°C, the ageing of the material is still accelerated, which consequently reduces its service time. Crosslinked polyethylene (PE) is one of the most common polymers used for cable insulation, and the presence of a crystalline phase combined with the crosslinking of amorphous chains provides stiffness and elasticity to the material. Compared to low comonomer content (~ 1wt%) PE, high comonomer content (~10wt%) PEcBs have a lower crystallinity and an enlarged and lower melting temperature domain, explaining their better flexibility, which is useful in many applications. PEcBs are designed to enable thermoplastic olefins to meet a variety of performances, especially in the areas of low temperature impact, melt flow, melt strength, flexibility, and softness. Polyethylene blends with different comonomer contents are mixed in the formulations of low voltage cables to bring an elastomer behaviour. Different ratios are used depending on the targeted properties, and offer the possibility to obtain softer materials which fulfill the required properties for applications in many domains, including automotive, ship building, rolling stocks, nuclear plants, photovoltaic modules as examples.

Thus, their combination with PE can offer a better compromise of the mechanical properties [1,2,3]. Nevertheless, the resistance of these materials to thermo-oxidation is another very important characteristic to consider when choosing the optimal formulation.

Different studies have shown that strong molecular modifications can occur during the thermo-oxidative ageing of PE with the formation of carbonylated and hydroxylated oxidation products [4,5,6], which lead to chain scission. Thus, the macromolecular architecture is strongly impacted [7,8], which, in combination with the influence of temperature on the crystalline morphology [9,10,11,12], has a strong influence on the mechanical behaviour [8,13,14]. Some studies have also reported that increasing the comonomer content increases not only the branching content (short chains branches) but also the oxidation rate [15,16]. In addition, when PE is crosslinked, chain scission modifies the architecture of the polymer network, and by

providing more mobility to the chains, they can promote an increase in the material crystallinity [17,18,19].

However, to the authors' knowledge, the evolution of crosslinked blends of low and high comonomer content PE during thermal ageing is much less documented, especially when considering the semi-crystalline microstructure, the network architecture and the mechanical properties evolution. Pospíšil et al.[20] reported that in polymer blends, co-reactivity of the degradation products of each polymer can occur. Blends are often more sensitive to degradation than pristine polymers [21,22,23,24]. One of the reasons may be the more complex semi-crystalline microstructure of the polymer, which can greatly change the relative position of the ageing temperature with respect to the melting temperature(s) of the crystalline phase. Indeed, it is known that crystallised chains are much more protected from oxidative degradation than amorphous chains [25],[26]. This aspect is particularly important in the case of the blends we studied in a previous work. In this study, we explored, at the molecular scale, the degradation mechanisms induced by thermo-oxidation in blends of two PEs with two different butene comonomer contents [4]. Three ageing temperatures (60°C, 90°C and 110°C) above or below the melting temperatures of PE or PEcB were studied. In particular, we showed that chemical analysis of degradation is not sufficient to determine the material durability since thermo-oxidative ageing leads to modifications of the semi-crystalline microstructure and elastomer network. Undoubtedly, both must be carefully studied because they directly impact the evolution of the mechanical properties. This is the aim of the present work, which is dedicated to studying the microstructure-property relationships of these blends before and after thermo-oxidative ageing.

2. Experimental section

2.1. Materials

Two linear polyethylene polymers, the first one with a middle comonomer content, hereafter called PE (LLDPE 324CE), was supplied by SABIC®, and the second one with a high monomer content, hereafter called PEcB (DF940), was supplied by TAFMER^{TM}. Both polyethylenes are copolymers of ethylene and butene, with 3.4% and 9.4% butene for PE and PEcB, respectively, as determined by ^{1}H and ^{13}C NMR spectroscopy [27] according to Nuanthanom's method [28]. The molar masses of both polyethylenes were measured by SEC (calibration was performed with polyethylene standards) and 1,2,4 trichlorobenzene as an eluent in a column at 150°C eluted at a flow rate of 0.6 mL/min, and the calculated masses were M_n = 20 000 g·mol^{-1} and

M_w = 73 000 g·mol^{-1} for PE and M_n = 22 000 g·mol^{-1} and M_w = 62 000 g·mol^{-1} for PEcB. Dicumyl peroxide (DCP, Arkema Luperox®) was used as a crosslinking agent.

2.2. Processing

PE/PEcB blends of 100/0, 70/30, 50/50, 30/70, and 0/100 wt% were prepared at the Nexans Research Center (Lyon). Pellets were processed in an external mixer at a temperature of 120°C and mixed with 2 wt. % DCP for 8 to 10 min. The crosslinking kinetics of the samples were determined using a Monsanto rheometer (Figure S1). The tests were carried out at 180°C, which is the decomposition temperature of DCP, a frequency of 100 Hz and a force of 11.0 ± 0.5 kN. Time t_{98} was defined as the time necessary to reach 98% of the maximum torque. Afterwards, the samples were calendered and then compression-moulded at 180°C under 200 bar for 6.5 min (t_{98}). Eighty-micrometre-thick films were obtained using moulds for spectroscopy analysis. Sheets with 400-500 µm thicknesses were used for other experiments (DSC, gel fraction, tensile tests, etc.). The composition of the different blends and the gel fraction of the crosslinked blends are listed in Table 1.

Table 1 – Composition and gel fraction of the blends.

Blend composition (wt. %)	Crosslinked samples*	Gel fraction (%)
100% PE	Per	88 ± 1
70% PE - 30% PEcB	7030r	88 ± 1
50% PE - 50% PEcB	5050r	85 ± 1
30% PE - 70% PEcB	3070r	89 ± 1
100% PEcB	PEcBr	89 ± 1

***including 2 wt. % DCP**

2.3. Thermal ageing

Thermo-oxidation of the samples was carried out in ovens with air circulation at three different temperatures: 60°C, 90°C, and 110°C. These temperatures were chosen to change the crystalline microstructure of the polymers during thermal ageing.

2.4. Characterization techniques

Differential Scanning Calorimetry (DSC)

A Mettler Toledo DSC 822 device was used to perform differential scanning calorimetry on 500 µm sheets heated from -20°C to 160°C at a heating rate of 10 °C/min under air flow.

Sample crystallinity was calculated from the heat of fusion using equation (1):

$$\chi\,(\%) = \frac{\Delta Hm}{\Delta Hm_{100\%}} \times 100 \qquad (1)$$

where χ is the crystallinity weight fraction, ΔH_m is the melting enthalpy of the semicrystalline sample and $\Delta Hm_{100\%}$ is the melting enthalpy of 100% crystalline PE, i.e., without considering the presence of defects along the polymer chain. $\Delta Hm_{100\%}$ is equal to 290 J/g [29]. Taking this value over the whole temperature range of measurements, we thus chose to neglect the slight variation of the melting enthalpy with temperature. The value of ΔH_m is deduced from the calculation of the area of the melting peak measured in the DSC curve. This peak is delimited by a baseline extrapolated from the DSC curve at temperature below and above those of melting. We have checked that these approximations should introduce an error below the experimental uncertainty (cf. figure 13 and 14), and should have therefore no incidence in the results discussion, which focuses on crystallinity evolutions. Given the very large temperature domain of melting of the materials studied, we however acknowledged that it would have been interesting to apply the methodology described in Gray et al. [30], which appears to be more adapted to this case. Moreover, for the same reason, complementary experiments by WAXS and density measurements could have been performed to confirm our DSC results. Thus, it must be emphasized for the reader that the crystallinity values used here are approximations and must not be taken as absolute values but as an indication of their evolution.

Small Angle X-ray Scattering (SAXS)

Small angle X-ray scattering (SAXS) experiments were carried out at the SWING beamline of the SOLEIL synchrotron (France). The measurements were performed using a wavelength of 0.77 Å, allowing for an observation range of q from 0.005 to 0.8 nm^{-1}. The SAXS patterns were recorded with a 2D detector. Each pattern was integrated azimuthally and corrected to eliminate background scattering. The corrected scattering intensity was normalized by the thickness and transmission of each sample. Finally, Lorentz-corrected scattering curves $I(q)q^2 vs. q$ were plotted. The one-dimensional correlation function $\gamma(r)$, calculated from the Fourier transformation of the Lorentz-corrected intensity, enabled us to obtain the structural parameters L_p, L_c and L_a by following the method described in [31]. $\gamma(r)$ is given by:

$$\gamma(r) = \frac{\int_0^\infty I(q) q^2 \cos(qr) dq}{Q} \quad \text{with} \quad Q = \int_0^\infty q^2 I(q) dq \qquad (2)$$

where *r* corresponds to the distance in the direction normal to the layer faces in the stack and *Q* is the scattering invariant.

From the structural parameters, the volumic crystallinity (χ_v) ratio can be calculated:

$$\chi_v = \frac{L_c}{L_p}$$

The relationship between χ (DSC) and χ_v (SAXS) is calculated thanks to ρ_c (1g/cm^3) and ρ_α (0,850/ cm^3) the bulk densities of crystalline and amorphous phases respectively:

$$\chi = \frac{\rho_c * \chi_v}{\rho_c * \chi_v + \frac{\rho_a}{\rho_c}(1 - \chi_v)}$$

The above relationship is only verified when the amorphous and crystalline phases are regularly distributed throughout the sample. For example, a semi-crystalline sample displays a usual spherulitic (or similar) microstructure, SAXS measurement enables to obtain intra-spherulitic crystallinity whose value will match with the one obtained by DSC measurement only if spherulites are contigous throughout the sample.

In our study, when the results of SAXS and DSC measurements don't match (when the temperature of measurement increases), it suggests that the microstructure is made of an amorphous phase in addition to the remaining un-melted semi-crystalline microstructure (all remaining spherulites are no longer contigous).

Gel fraction

The gel fraction was measured by refluxing polymers in boiling p-xylene at 140°C for three days and subsequently drying in a vacuum oven at 60°C for two days. The gel fraction was calculated by dividing the remaining mass by the original mass of the polymer introduced in the refluxing system. Three pieces of the same sample were introduced at the same time to ensure the reproducibility of the measurement.

Tensile tests

Tensile tests were performed on an MTS device with a temperature-controlled chamber. Experiments were carried out at 25°C and 130°C (above the crystallite melting temperature of both polyethylenes) with a 0.01 s^{-1} nominal strain rate. The samples were dumbbell-shaped with typical dimensions of 12 x 4 x 0.5 mm^3. For each material, two specimens were tested. The Young's modulus E was calculated as the slope at the origin of the nominal strain–stress curve. The elastically active chain (EAC) density ν was deduced from the modulus measured from stress-strain curves obtained at 130°C with equation (3) by assuming an affine description of the entropic elasticity:

$$E = 3\nu kT \quad (3)$$

where k is the Boltzmann constant and T is the temperature (K).

Scanning Electron Microscopy (SEM)

SEM micrographs were recorded using a ZEISS Supra 55VP scanning electron microscope (property of the Consortium Lyon St-Etienne de Microscopie platform) operating under high vacuum at 1 kV. A secondary electron detector (Everhart-Thornley detector) was used. The microscope was equipped with a Gemini column working at low voltage so that nonconducting samples could be observed without any surface preparation. These operating conditions enables to better detect the morphological details of the semi-crystalline microstructure of the studied polymers.

Polymer sheets were fractured in liquid nitrogen and installed between two metallic folds to observe the film cross sections.

Transmission Electron Microscopy (TEM)

TEM micrographs were recorded using a Philips CM120 microscope (Centre Technologique des Microstructures of Université Lyon 1 platform) operating at 120 kV with a GATAN Orius 200 2Kx2K lateral camera from CTμ. Polymer sheets were ultramicrotomed at -150°C (Leica UC7 equipped with a cryo unit) to obtain films with a thickness of approximately 100 nm, which were deposited on 400 mesh copper grids.

3. Results

3.1. Part 1: Characterization of polymers and blends before ageing

3.1.1. Morphology

Figure 1 shows the cross-sectional SEM images (secondary electron) of PEr, PEcBr and the 5050r blend before ageing (images of the two other blends are reported in Figure S2). All the samples show a homogeneous morphology at the observation scale. The fracture is fragile for all the materials except PEcBr. This material has a high butene content and therefore a lower crystallinity and a lower fraction of amorphous phase confined between lamellae. The main fraction of its amorphous phase is therefore mobile enough to relax part of the macroscopic deformation imposed during cryofracture. For all the samples except PEcBr, the micrographs show small cavities where the fracture initiates. Lamellae blocks radiate from this cavity, suggesting the existence of a macroscopic spherulitic structure, as already observed in LLDPE with similar comonomer content and crystallinity [32]. Despite the low PEr content in the 3070r blend, which strongly reduces the crystallinity (cf. table 2), some cavities surrounded by smaller spherulitic structures are still visible. Thus, the crosslinking by 2% DCP did not inhibit the formation of these morphologies.

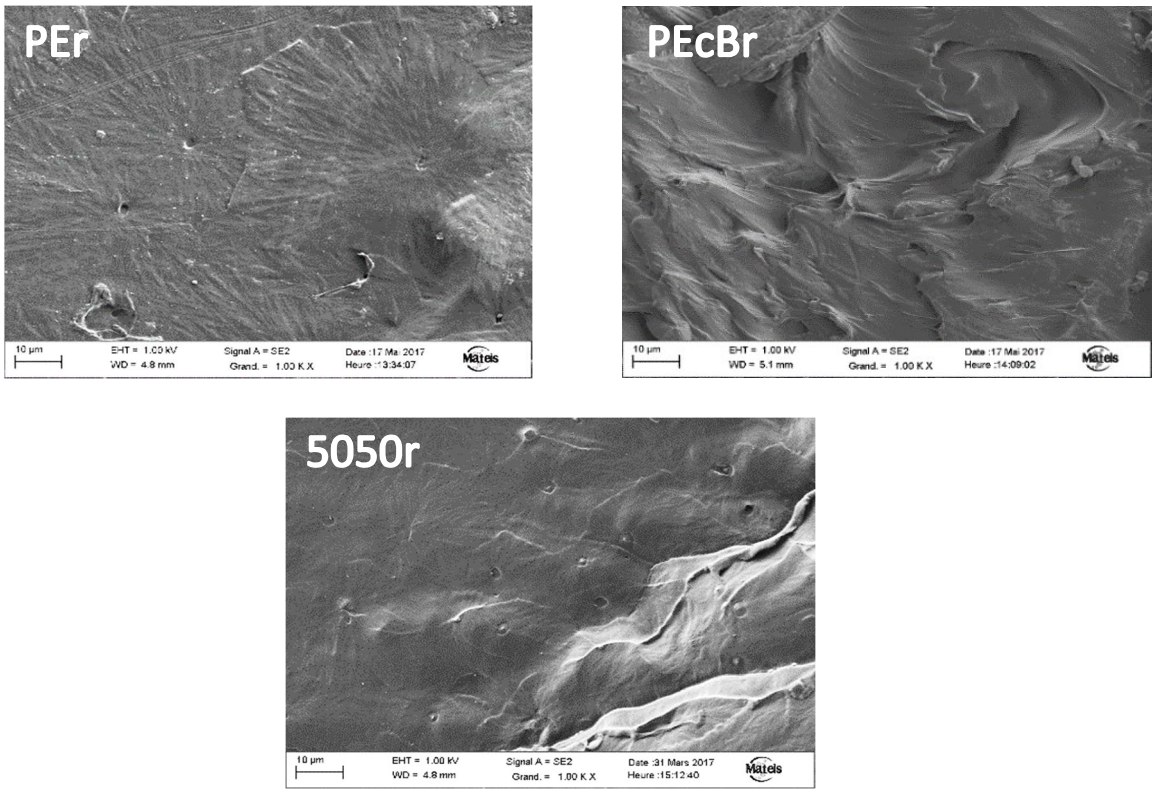

Fig. 1. Cross sectional SEM images of PEr, PEcBr and 5050r before ageing (secondary electron, low voltage conditions).

The TEM micrographs of the five cryo-microtomed formulations (cf. Figure 2 and Figure S3) show the morphology observed by SEM at a smaller scale. The images confirm in PEr the

complex crystallites lamellae organisation inside the spherulites, as classically observed in the literature for PE [33,34,35] and LLDPE [32,36,37]. Such a structure is not observed in PEcBr, whose TEM image suggests the presence of a “bundle-like” granular morphology, with so-called fringed micellar crystals [36, 39, 45]. The 5050r, 7030r and 3070r blends present an intermediate morphology. At last, like the SEM images, the TEM images of the blends do not show any obvious phase segregation that could suggest the partial immiscibility of the two polyethylenes at the micron scale.

It was not in the objective of this work to go further in the observation by microscopy even though much more work could be conducted to try to have more information on the materials microstructure. For instance, microscopy could be performed on well controlled samples preparation using etching, replica techniques…to enhance the lamellar contrast, which enable, when properly performed, to estimate lamellae thicknesses and spacing [35]. At a larger scale, cross polarization microscopy may also reveal superstructure (even though our first attempts was however unsuccessful). We therefore acknowledge that our interpretation is based on a small amount of experimental data, and that it would therefore be interesting to confirm with additional experiments .

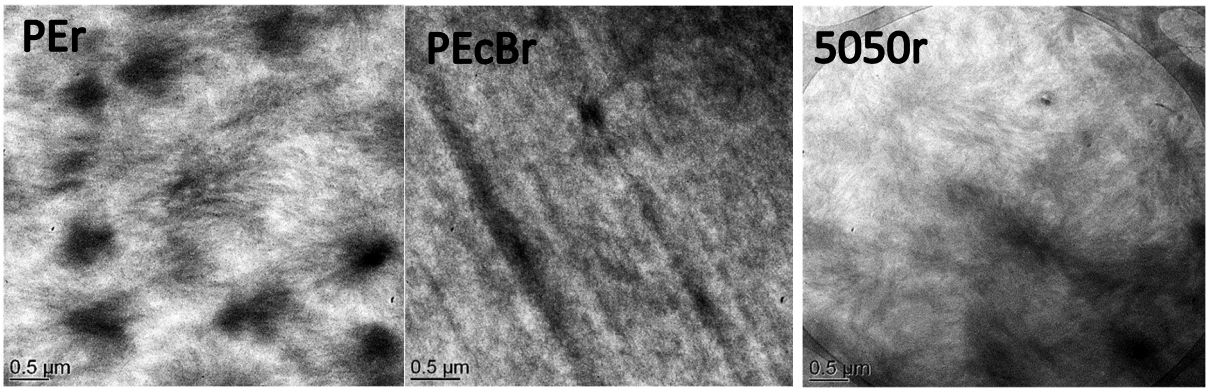

Fig. 2. TEM images of the microtomed PEr, PEcBr and 5050r blend before ageing.

3.1.2. Microstructure

Preliminary DSC characterization is presented in reference [4]. The DSC thermogram of PEr displays a classic shape, with a sharp melting peak at 115°C superimposed with a very large peak spread over lower temperatures corresponding to the melting of the smallest crystallites

[19]. The deduced PEr crystallinity was equal to 40%. The DSC thermogram of PEcBr displays two melting peaks at 45°C and 78°C, which are related to two different types of crystals, as usually found for PEs in ethylene-octene copolymers [32,37,38,39,40,41] and ethylene-butene copolymers [42,43] with large amounts of comonomers. The high-temperature part of the melting peak can be attributed to PE-like crystals with a lamellar morphology, while the lower-temperature endothermic region may correspond to fringed micellar or "bundle-like" smaller crystals. The crystallinity of unaged PEcBr is equal to 25%, which is lower than that of PEr, as already observed in the literature [39,40]. Indeed, its higher comonomer content reduces its ability to crystallize by shortening the length of crystallizable ethylene sequences.

Figure 3 shows the DSC thermograms of the 7030r, 5050r and 3070r blends in comparison with the curves computed from a weighted summation (using the weight fraction of each polymer) of the curves of PEr and PEcBr polymers.

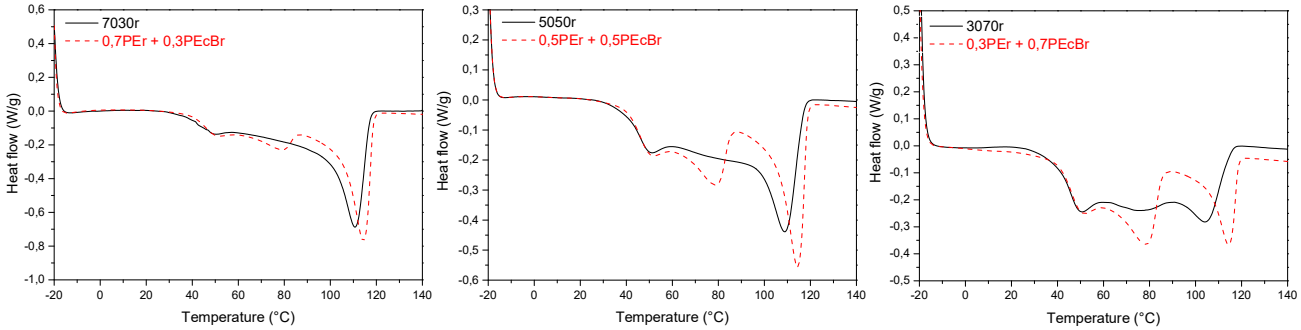

Fig. 3 - First DSC heating step for the 7030r, 5050r and 3070r blends (the dashed line shows the weighted summation of the experimental heating scans of the individual polymers using their weight fraction in the blend).

The heating curve of the blend displays two melting endotherms that roughly correspond to the two individual polymers. This indicates the existence of phase separation *at the scale of the crystallite size*, meaning, as expected, that PEr and PEcBr are not fully miscible. Moreover, the main melting temperature of PEr crystals in the blends is lower than that measured in pure PEr, indicating that their thickness is smaller [44,45,46]. In addition, the melting endotherm at approximately 80°C, ascribed to PEcBr crystals, systematically has a lower amplitude than the endotherm measured in pure PEcBr, suggesting that PEcBr chains are missing in the PEcBr-rich crystal phase of the blends. In addition, the endothermic signal recorded in the temperature range between the low- and high-temperature endotherms of the blends is higher in intensity in

the experimental curves than in the computed curves. This suggests the presence of a significant amount of PE and PEcB cocrystals.

Figure 4 shows, as an example, the SAXS profiles of PEr (without thermal ageing) measured at different temperatures, with a peak whose maximum position slightly decreases with increasing measurement temperature. Table 2 reports the long period L_p and the corresponding lamellar thickness L_c deduced from the γ(r) plot.

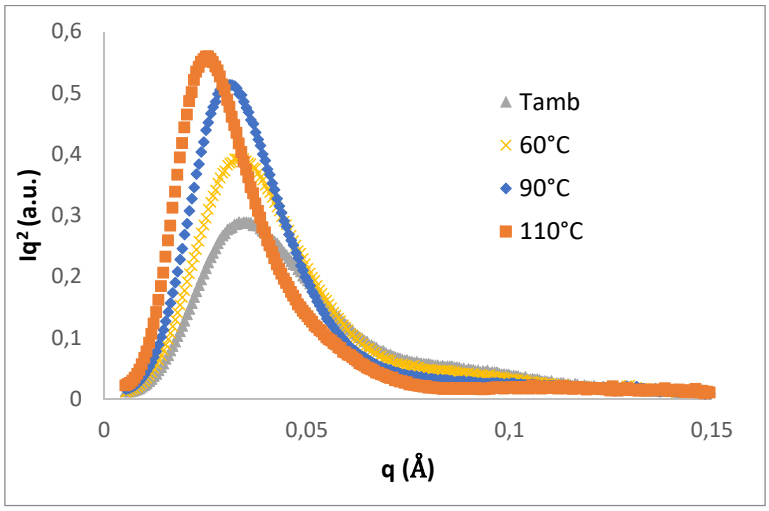

Fig. 4. SAXS profiles of PEr (without thermal ageing) measured at ambient temperature, 60°C, 90°C and 110°C.

Table 2 – L_p (nm) and L_c (nm) measured from the SAXS profiles of PEr, PEcBr and 5050r. Numbers are written in italics when the SAXS profile displays several peaks, which makes the calculation of Lp and Lc from the autocorrelation function γ(r) questionable.

	PEr				**5050r**				**PEcBr**			
	L_p nm	**L_c nm**	**X_v SAXS vol.%**	**X_c DSC wt.%**	**L_p nm**	**L_c nm**	**X_v SAXS vol.%**	**X_c DSC wt.%**	**L_p nm**	**L_c nm**	**X_v SAXS vol.%**	**X_c DSC wt.%**
T_{amb}	16.4	5.7	35	40	12.4	4.1	33	32	10.5	3.7	35	25
60°C	16.9	5.7	34	36	14.5	4.8	33	25	13.7	4.1	30	15
90°C	18.5	6.5	35	28	***20.1***	***5.7***	28	14	-	-	-	-
110°C	22.5	7.3	32	11	***27***	***6.5***	24	1	-	-	-	-

When the measurement temperature is increased (60°C and 90°C), the long period L_p and Lc slightly increase. As expected, X_c calculated from the DSC results significantly decreases. Increasing the temperature leads to the melting of increasingly thick crystallites. Nevertheless, the limited variation in L_p and the very limited variation in X_v deduced from SAXS suggest that the thickest crystallites are regrouped together in domains. Note that it is, however, difficult to know where the small crystallites are located, as they could be part of the spherulites or localized outside of them.

Regarding PEcBr, at T_{amb}, its long period and crystallite thickness are smaller than those of PEr (cf. Figure S4 and Table 2). The larger width of the correlation peak indicates a larger L_p distribution related to a larger thickness distribution of both the amorphous layers and the crystal lamellae, which are in agreement with the DSC result and the literature [39,47,48,49,50]. At 60°C, when PEcBr is partially molten, L_p and L_c increase (slightly), which corresponds to a reduction in the distribution of the crystallite thickness by the melting of the smaller crystals. The reduced change in Xv deduced from SAXS (as maybe the TEM image) again indicates that the different crystallite populations are regrouped in domains.
The L_p and L_c values were also calculated from the SAXS experiments for the different blends. These calculations must, however, be considered with caution at 90°C and 110°C, as the SAXS profiles reveal a bimodal distribution. Values are reported in Table 2 for the 5050r blend, and reported as supporting information for the other blends (Table S1, Figures S5-S7). Their values are between those of PEr and PEcBr and therefore consistent with the DSC data.

3.1.3. Mechanical properties

The nominal stress-strain curves at 25°C of the five unaged materials are reported in Figure 5. In contrast to what is observed with uncrosslinked PE [56], no necking was observed for the different materials at the beginning of plastic deformation. The high modulus of uncrosslinked PE is related to the formation of a percolated crystalline network that is strongly linked by tie molecules. The more numerous these molecules that transmit stress between lamellae are, the more homogeneous the distribution of these stresses, and the less localized deformation [56]. Following this idea, in PEr, the crosslinks rejected from the crystalline phase increase the number of “stress transmitters” and therefore homogenize material deformation. In PEcB, regardless of whether it is crosslinked or not, numerous and small crystallites act as homogenously distributed crosslinks. As expected, both the elastic modulus and yield stress decrease with increasing PEcB content as a result of the lower degree of crystallinity of the

materials and the lower thickness and perfection of the crystallites (which are less resistant to plastic deformation) [51, 52].

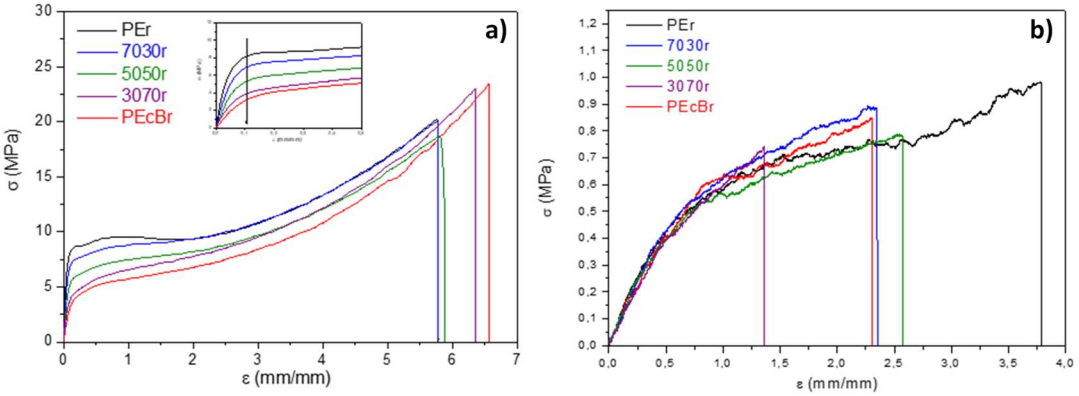

Fig. 5. a) Stress-strain curves at 25°C of the two polymers and the three blends before ageing. b) Nominal stress-strain curves at 130°C for the two polymers and the three blends before ageing.

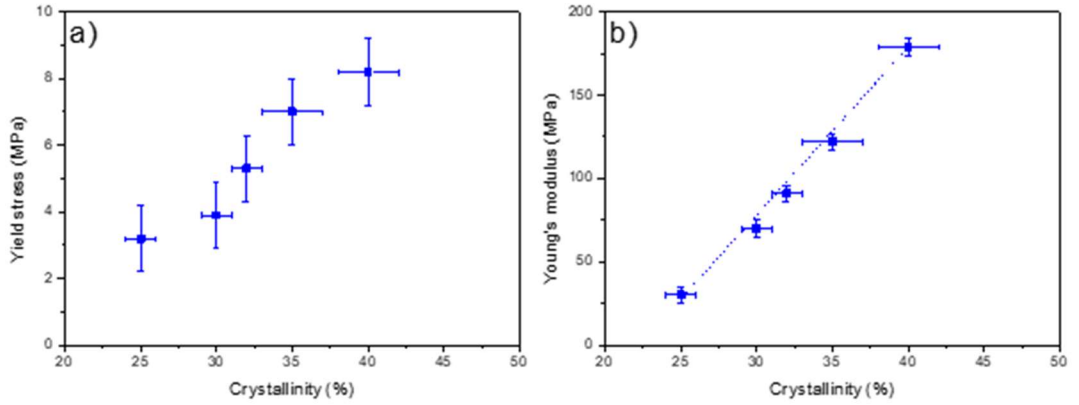

Fig. 6. a) Yield stress and b) Young's modulus plotted vs crystallinity.

A very linear relationship is found between the modulus and the crystallinity (cf. Figure 6), which agree with the data of the literature [53,54,55,56,57]. The strain hardening is very similar for the five materials, and at large strains, a very similar stress level is measured regardless of the PEcBr content. Thus, deformation seems to eliminate the influence of the crystalline morphology, and the material behaves as a highly crosslinked and reinforced elastomer at large strain. Note the slight increase in the elongation at break with increasing PEcBr content in the blends. This is expected, as less crystallite shearing is a priori necessary to obtain a large strain level [18,39,58,59].

The nominal stress-strain curves, obtained at 130°C, are plotted in Figure 5b. Considering that the reproducibility of the elongation at break was not good enough, the rupture behaviour of the samples will not be discussed, and the interpretation will be focused on the elastic modulus. The testing temperature is much higher than the melting temperature of the crystallites of both polyethylenes. Moreover, this temperature is much higher than the glass transition temperature of the polymer chain, and the contribution of the free entanglements and pending chains can also be neglected in the mechanical response. Thus, the observed behaviour is significant for the elastic network architecture (formed by the chemical crosslinks and the trapped entanglements). The unaged polymers and blends display the same Young's modulus (ca. 1 MPa) at 130°C. This corresponds to an elastically active chain (EAC) density of ca. 1.0×10^{-4} $mol\cdot cm^{-3}$. Considering that the density of both polyethylenes is approximately $\rho = 0.9$ $g\cdot cm^{-3}$ and that the molar mass between entanglements is ca. $M_e = 1200$ $g\cdot mol^{-1}$, the deduced subchain density between entanglements should be $\nu_e = \frac{\rho}{Me} \approx 7.5\ 10^{-4}$ $mol\cdot cm^{-3}$. Given the large molar weight of the initially uncrosslinked PE and PEcB chains (M_n approximately 20 000 $g\cdot mol^{-1}$), the crosslinked samples should contain a very significant amount of trapped entanglements. Thus, the elastically active chains of the crosslinked homopolymers and blends are mainly created by these trapped entanglements. The significant soluble fraction reported in Table 1, ca. 10%, can therefore be explained by the relatively low chemical crosslink density, which is identical regardless of the PEcB content, and the relatively large polymolecularity index (above 3), which leads to a significant amount of uncrosslinked short chains.

3.2. Part 2: consequences of thermal ageing

As mentioned in the introduction, the studied polymers and blends, before and after ageing, have already been chemically characterized in a previous article (by using infrared and UV-visible spectroscopy techniques) [4]. The thermo-oxidation mechanism of both polyethylenes was confirmed by performing chemical derivatization. The non-Arrhenius evolution of the measured concentration of the degradation products in the aged materials in the [60°C;110°C] temperature domain was also evidenced, which could not be explained by the physical state of the polymers, i.e., the global crystallinity at the chosen ageing temperature. The following characterization completes these results and focuses on the evolution of the network architecture and the semi-crystalline microstructure of the materials.

3.2.1. Morphology

SEM images of the cryo-fractured surfaces of PEr, PEcBr and 5050r after ageing at 110°C for 100 h are reported in Figure 7 (images for 7030r and 3070r are in Figure S8). The SEM images of PEr and PEcBr are very different, with the SEM images of the blends being intermediate, due to the differing contents of each PE. For the PEr and 7030r samples, which showed spherulites morphology, after thermal degradation (especially at 110°C), the spherulites seem to be fractionated in smaller domains surrounded by a ductile phase. As the PEcBr content increases, degradation leads to the observation of numerous and thin ductile zones on the cryo-fractured surface. These results could be ascribed to the accumulation of polar oxidation products in the amorphous phase of the polymer [13,14]. Note that as already acknowledged in section 3.1.1, our interpretations are based on a small amount of experimental data. It would therefore be interesting to confirm it with additional experiments .

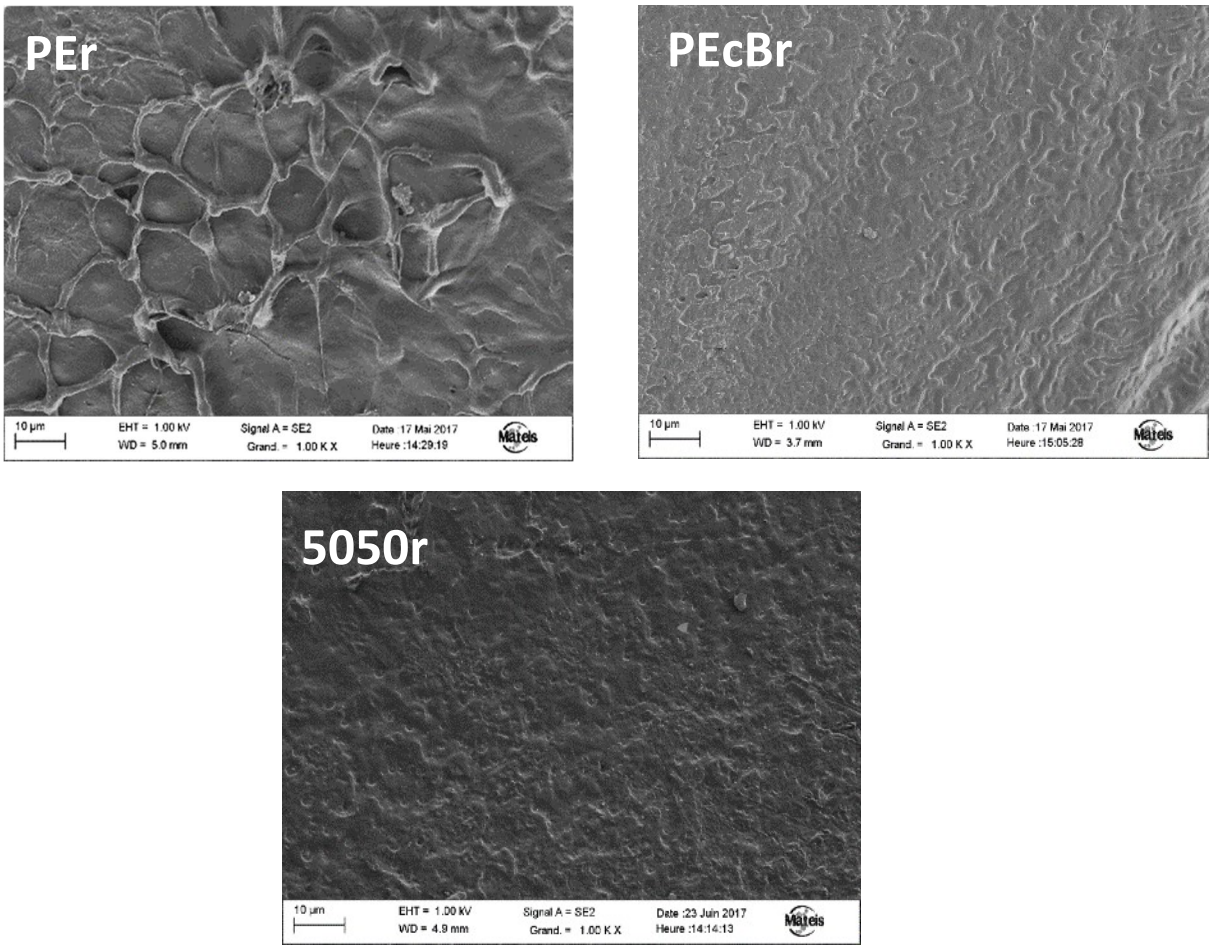

Fig. 7. Cross-sectional SEM images of PEr, PEcBr and the 5050r blend recorded after 100 h of thermal oxidation at 110°C.

3.2.2. Microstructure

DSC thermograms of PEr thermo-oxidized at 60°C, 90°C and 110°C for several ageing durations are presented in Figure 8. The deduced melting temperatures (taken at the maximum of the peak) and crystallinity are listed in Table S2. Regardless of the ageing temperature, a "digging" of the melting endotherm at the ageing temperature and the formation of an additional endothermic peak above this temperature are observed. The main melting temperature of PEr remains constant, except for ageing at 110°C, where it increases with ageing duration due to the proximity of the ageing temperature to the one of the main melting peaks. This "digging" is ascribed to lamellar thickening, i.e., the chains of the molten crystals at the ageing temperature can be recrystallized with time and incorporated into thicker crystallites whose melting temperature is just above the ageing temperature.

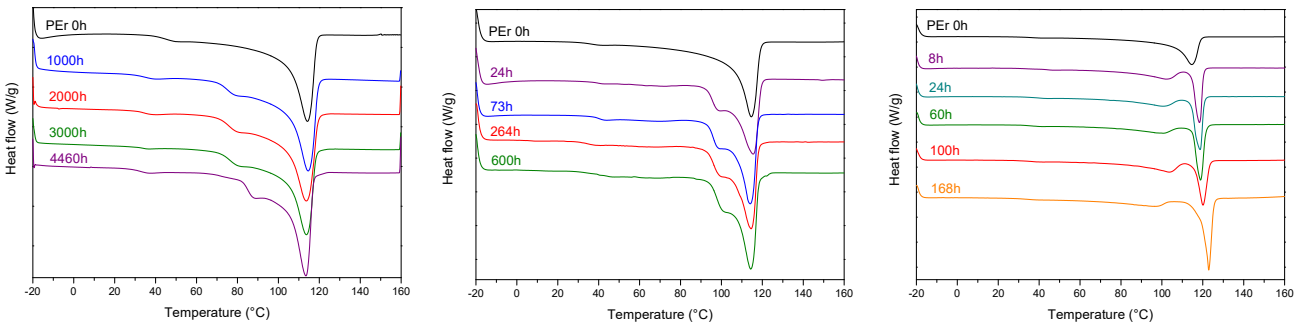

Fig. 8 – Heat flow during the first DSC heating step of PEr after thermo-oxidation at 60°C (left), 90°C (middle) and 110°C (right).

The SAXS data measured at 60, 90 and 110°C (cf. Table 3) do not show a significant impact of ageing at 60°C on the crystallite characteristics. For ageing at 110°C (unfortunately, we did not perform measurements for ageing at 90°C), lamellar thickening was confirmed, as both L_p and L_c slightly increased (Figure S9 and Table 3). This annealing process has already been reported in the literature [10,12,19]. Moreover, the increase in the overall crystallinity of PEr means that amorphous chains are also incorporated into crystallites. This process should be facilitated by chain scission, which provides more mobility to the polymer chains, i.e., chemi-crystallization may occur. The small increase in the gel fraction of the materials (see further), however, indicates that this phenomenon is weak.

Table 3 – L_p (nm) and L_c (nm) deduced from the SAXS profiles measured at Tamb, 60°C, 90°C, and 110°C (in supporting information) before and after ageing PEr.

	Ambient T		60°C		90°C		110°C	
Ageing	**L_p (nm)**	**L_c (nm)**	**L_p (nm)**	**L_c (nm)**	**L_p (nm)**	**L_c (nm)**	**L_p (nm)**	**L_c (nm)**
none	16,4	5,7	16,9	5,7	18,5	6,5	22,5	7,3
3000 h at 60°C	14,5	5,7	15,5	5,7	18,8	6,5	22,5	7,3
60 h at 110°C	18	6,1	18	6,1	20,1	6,9	25,7	8,1

Because the complete melting temperature of PEcBr is below 90°C, the consequences of ageing on the microstructure are different when it is performed at 60°C, on the one hand, or at 90°C and 110°C, on the other hand (cf. Figure 9 and Table S3). After ageing at 60°C, similar to PEr, the evolution of the DSC thermograms (Figure 9) indicates that annealing occurred. This corresponds to a slight increase in Lp and Lc deduced from SAXS (cf. Table 4). Conversely, ageing at 90°C and 110°C does not lead to a significant modification of the thermogram. This thermogram is that of a sample in which the thermal history of the crystalline microstructure has been erased by heating at the ageing temperature. This is confirmed by the unchanged SAXS profiles (measured at Tamb and 60°C; cf Figure S10 and Table 4). Note also that even at the longest ageing durations, which corresponds to a degraded material, the crystallinity ratio is not modified, in contrast to what was observed for PEr.

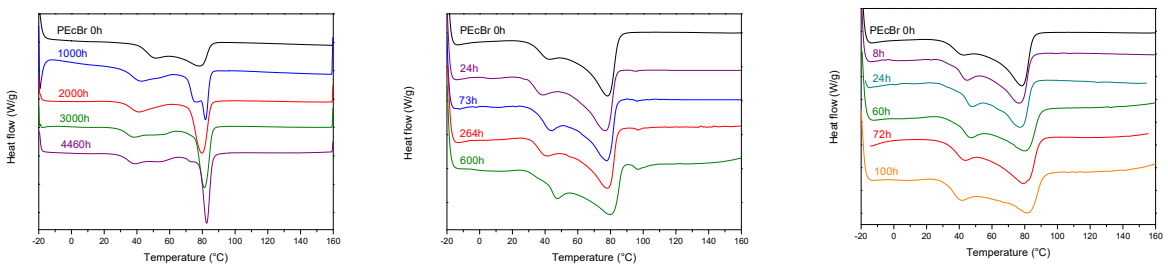

Fig. 9. Heat flow during the first DSC heating step of PEcBr after thermooxidation at 60°C (left), 90°C (middle) and 110°C (right).

Table 4 – L_p (nm) and L_c (nm) measured from the SAXS profiles of PEcBr before and after thermooxidation.

Measured at	Ambient T		60°C	
	L_p (nm)	L_c (nm)	L_p (nm)	L_c (nm)
Before ageing	10,5	3,7	13,7	4,1
After 3000 h at 60°C	11,3	3,7	14,5	4,1
After 100 h at 110°C	10,5	3,7	13,7	4,1

The DSC thermogram evolution of the blends after ageing at 60°C, 90°C and 110°C roughly corresponds to the combination of the ones of each homopolymer, in relation to their volume fraction. (cf. Figure 10 and Table S4 for 5050r, Figure S11 and Table S5 for 7030r, and Figure S12 and Table S6 for 3070r). Thus, lamellar thickening is also observed, especially in the first steps of degradation, and leads to an increase in the crystallite population whose melting temperature is just above the ageing temperatures. This phenomenon is promoted by the initial presence of crystallites whose melting temperature is just below the ageing temperature. This explains why this phenomenon is particularly visible with the 5050r materials, regardless of whether they are aged at 60°C or 90°C. Moreover, as expected, the higher the content of PEr is, the larger the increase in crystallinity (especially for ageing at 110°C), which may be partly due to chemi-crystallization at long ageing times. In agreement with the nul or the slight evolution of the SAXS profile of PEr and PEcBr after ageing at 60°C, respectively, the evolution of the SAXS profile of the blends can be considered negligible for this ageing condition. The influence of the PEcBr content on the SAXS profiles of the blends after thermal ageing at 110°C (Figure S16) is consistent with its impact on the initial crystalline microstructure. Nevertheless, the obtained profiles are complex, as they are related to the scattering of different crystallite populations that evolve or not, depending on the closeness of their melting temperature to the ageing temperature (Figure S13, Figure S14 and Figure S15 for 7030r). For this reason, the estimate of L_p and L_c may be very hazardous: even though some values have been calculated and reported in the SI, they will not be further discussed.

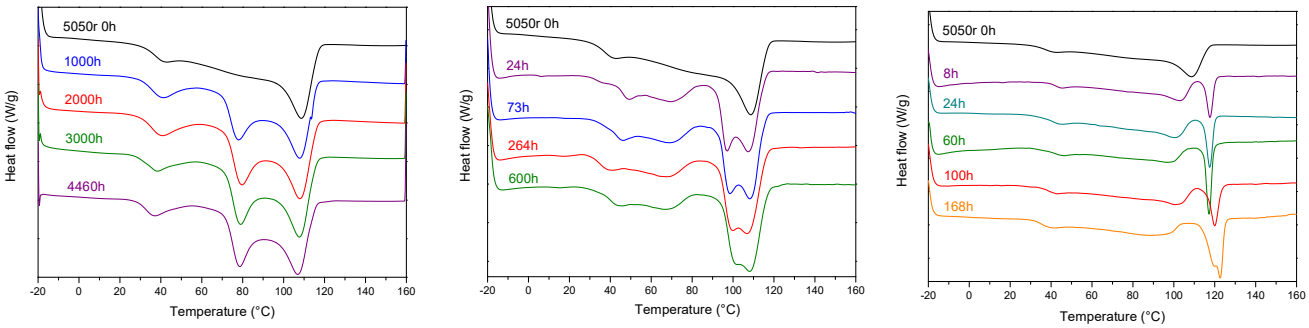

Fig. 10. Heat flow during the first heating DSC step of the 5050r blend after thermooxidation at 60°C (left), 90°C (middle) and 110°C (right).

3.2.3. Macromolecular architecture

A decrease in the gel fraction of the samples is observed after thermo-oxidation at 60°C, 90°C and 110°C, and is stronger as the ageing temperature and PEcBr content increase (cf. Figure 11). Chain scission is therefore the preponderant mechanism [15, 16,59]. However, the decrease in the gel fraction is much smaller in the case of the samples thermo-oxidized for 3000 h at 60°C, likely because the degree of the advancement of oxidation reactions (given the chosen ageing times) is lower than that of the samples thermo-oxidized at 90°C and 110°C. Moreover, the ageing mechanism at high temperatures might not be the same as that at lower temperatures [4]. For long ageing times at 90°C and 110°C, the rapid decrease in the gel fraction is concomitant with the previously reported significant increase in crystallinity, supporting the previous assumption of the occurrence of chemi-crystallization. However, this phenomenon only becomes significant for the longest ageing time, and the modifications of the microstructure at the shortest time are mainly the results of crystallization kinetics being accelerated by the ageing temperature. The EAC densities deduced from the measured Young's modulus at 130°C are reported in Figure 12. Regardless of the ageing time and temperature, the deduced EAC density of the materials is found to be lower than their initial density, confirming the preponderance of chain scission.

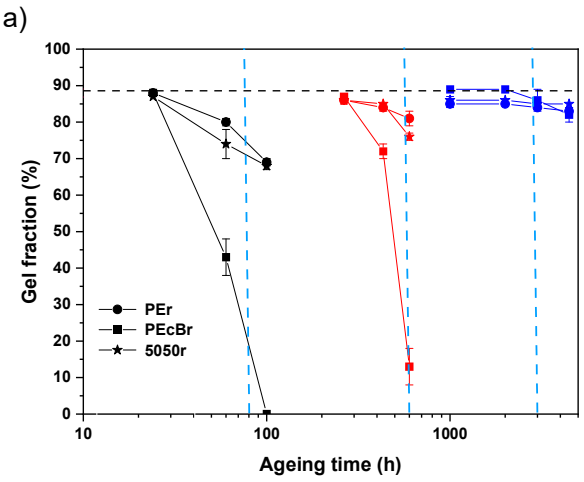

Fig. 11. Gel fraction plotted vs. ageing time at the three ageing temperatures: 60°C (blue curves), 90°C (red curves) and 110°C (black curves) for PEr (●), 5050r (★), and PEcBr (■) The horizontal dotted black line represents the gel fraction before ageing.
The vertical dotted lines are plotted at the chosen ageing time for the tensile tests at 130°C.

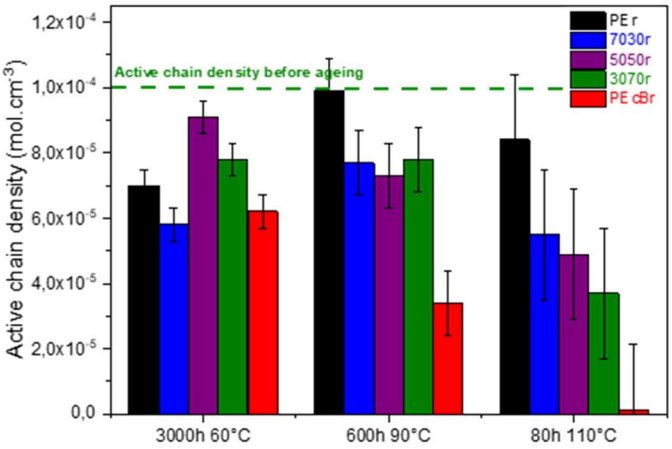

Fig. 12 – Elastically active chain (EAC) density of the two polymers and the three blends in the amorphous state before and after thermal ageing at 60°C, 90°C and 110°C, as deduced from the Young's modulus measurements at 130°C.

4. Discussion

As shown in Figure 12, the modifications by ageing of the EAC density (measured at 130°C in the amorphous state) and of the gel fraction of the molten blends cannot be easily predicted from those of the homopolymers. For instance, after ageing for 3000 h at 60°C, one observes

the smallest decrease in the EAC density for 5050r, whereas it changes more significantly for both homopolymers. This suggests that EAC network modification may also be related to the crystalline microstructure during ageing. It is important to recall that the largest crystallites are likely made of the largest PE sequences. By reducing the ageing temperature or by increasing the PEcB content, the distribution length of the crystallized EAC is shifted towards smaller values. During ageing, this promotes the scission (as this is the main degradation mechanism here) of the shortest EAC. Nevertheless, scission of a short EAC is less efficient in increasing the sol fraction, as the probability of cutting them several times is reduced. Cutting short EACs instead of long ones is also less efficient in decreasing the modulus when a large part of this modulus is the consequence of the trapped entanglements of the longest EACs. This fact is particularly important in this study, as the main fraction of the crosslinks are these trapped entanglements. Moreover, the consequences of EAC scission on the modulus also depend on the spatial distribution of EACs. It should be more important if the cut EAC creates a percolating soft phase.
This interpretation grid can be applied to our experimental results.

Let us first consider the material network evolution after 3000 h of ageing at 60°C. The modulus measured at 130°C and the deduced averaged EAC density of PEr are significantly decreased. Given the important crystallinity of the materials during ageing (initially 36%, with an increase up to 44% due to annealing), chain scission mainly occurred in the shortest EAC. The longest EACs were protected by crystallization and can still contribute to the EAC network. This explains the still low soluble fraction of the aged materials. After ageing, 7030r has a slightly lower EAC density than PEr. This may be explained by the significantly lower crystallinity of this material during ageing (36% after ageing at 60°C for 1000 h) and by the larger content of PEcb, which promotes chain scission. Nevertheless, the results obtained for 5050r do not follow the trend: its average EAC density (and modulus at 130°C) is very slightly reduced after ageing (3000h at 60°C). The different morphology of 5050r compared to that of PEr and 7030r can provide an explanation. As suggested by the SEM images (Fig. 7), in PEr materials, because of their spherulitic structure, degradation should be more heterogeneous and create a percolating soft phase. Mechanically, this is more efficient in decreasing the modulus (and therefore, the deduced *averaged* EAC density at 130°C) than a more homogeneous spatial distribution of cut chains. In contrast to PEr and 7030r, 5050r does not have spherulitic structures, making its degradation more homogeneous. This is consistent with the fact that the soluble fractions of PEr and 5050r are close despite their different moduli at 130°C, since the soluble fraction does

not depend on the localization of the free chains in the material. Logically, increasing the PEcB content (3070r and PEcBr) leads to materials being more sensitive to degradation than 5050r. This cannot be compensated by supplementary modifications of the morphology, as these ones are not as important as those observed when comparing 7030r and 5050r. Fewer EACs can be protected from scission as the crystallinity decreases, down to 26% for 3070r and 18% for PEcBr. However, the protection of the longest EAC by crystallization is sufficient to still inhibit a large increase in the soluble fraction.

During ageing at 110°C, the remaining crystallinity at this temperature is much less important than that at 60°C, especially for a large PEcBr content (it is even null in PEcBr), and the influence of the semi-crystalline microstructure on material degradation is strongly reduced. Therefore, as expected, the decrease in modulus at 130°C and decrease in gel content are more important when the PEcB content increases. The results obtained after ageing at the intermediate temperature of 90°C are consistent with all our analyses. At this temperature, a significant crystallinity remains in the materials during ageing (except in PEcBr). Thus, the difference in morphology induced by the increase in PEcB content may partly attenuate the impact of this increase on both the global material crystallinity (which decreases) and the sensitivity to thermo-oxidation (which increases).

Effects on the mechanical properties at ambient temperature: Nominal stress-strain curves of the different samples, unaged, aged for 600 h at 90°C, and aged for 80 h at 110°C, are reported in Figure 13. For clarity, the stress-strain curves of the same samples aged for 3000 h at 60°C are reported in Figure S17. A quasi-linear relationship is found between the Young's modulus and the crystallinity of the unaged materials, as shown by the trend curve plotted in Figure 14. Regarding the PEr data, ageing at 110°C causes degradation of the network made of initially amorphous chains and the molten (initially crystalline) phase. When cooled after ageing, a large amount of the degraded phase recrystallizes (including initially non-crystallized polymer). The formed crystallites create new links between the chains, thus partly compensating for the network degradation and the destruction of the tie molecules joining crystallite lamellae. The new crystalline microstructure is, however, slightly less mechanically efficient than the initial microstructure for reinforcing the polymer (as the same modulus is obtained for a larger crystallinity). During ageing at 90°C, the PEr crystalline phase is, for a large part, not molten, and more lamellar thickening occurs. After cooling to ambient temperature, a large fraction of the crystalline material is made of crystallites that melt above the ageing temperature (their fraction increased at the beginning of ageing by lamellae

thickening). Despite the resulting larger crystallinity, the modulus of PEr decreases as chain scission decreases the density of tie molecules between crystallites. The explanation is globally the same for the consequences of ageing for 3000 h at 60°C. The difference lies in the fact that at 60°C, most of the initially crystalline phase is not molten and that chain scission mainly occurs in shorter PE chains rejected from the spherulitic crystalline structure.

PEcBr is completely molten during ageing at 90°C and 110°C. Thus, even when a significant amount of chains has been cut, recrystallization at ambient temperature enables the reformation of a crystalline microstructure with tie molecules and thus limits the modulus decrease. During ageing at 60°C, PEcBr is only partially molten, and lamellar thickening also occurs. Moreover, network degradation is less important after 3000 h than after 80 h at 110°C; nevertheless, the modulus measured at ambient temperature is significantly lower. Thus, recrystallization at ambient temperature of the partially molten crystalline phase during ageing is seemingly less efficient at compensating for network degradation than complete recrystallization of the completely molten polymer, as the newly created tie molecules are much more numerous in this latter case. This is consistent with the previous observations on PEr.

As shown in Figures 13 and 14, the behaviour of the blends is intermediate between that of PEr and that of PEcBr, depending on the PEcB content. For them, the consequences of ageing strongly depend on the temperature, as this will more or less lead to the melting of the initially present crystalline phase and, consequently, more or less recrystallization. This will therefore more or less compensate for the decrease in the average EAC density. Note, however, the nonmonotonic evolution of the crystallinity with the PEcB content after ageing at 90°C, which is likely related (i) to the different ratios of molten and crystalline phases at this temperature for the 5050, 7030 and 3070 blends and (ii) to the ability of the molten phase undergoing chain scission, on the one hand, to participate in the annealing process and, on the other hand, to recrystallize at ambient temperature. As a consequence, 5050r has a lower crystallinity than 3070r and 7030r. However, because its modulus at 130°C is close to that of these two materials and its intermediate morphology (between spherulitic and fringed micellar morphologies), i.e. its semi-crystalline microstructure is more mechanically efficient.

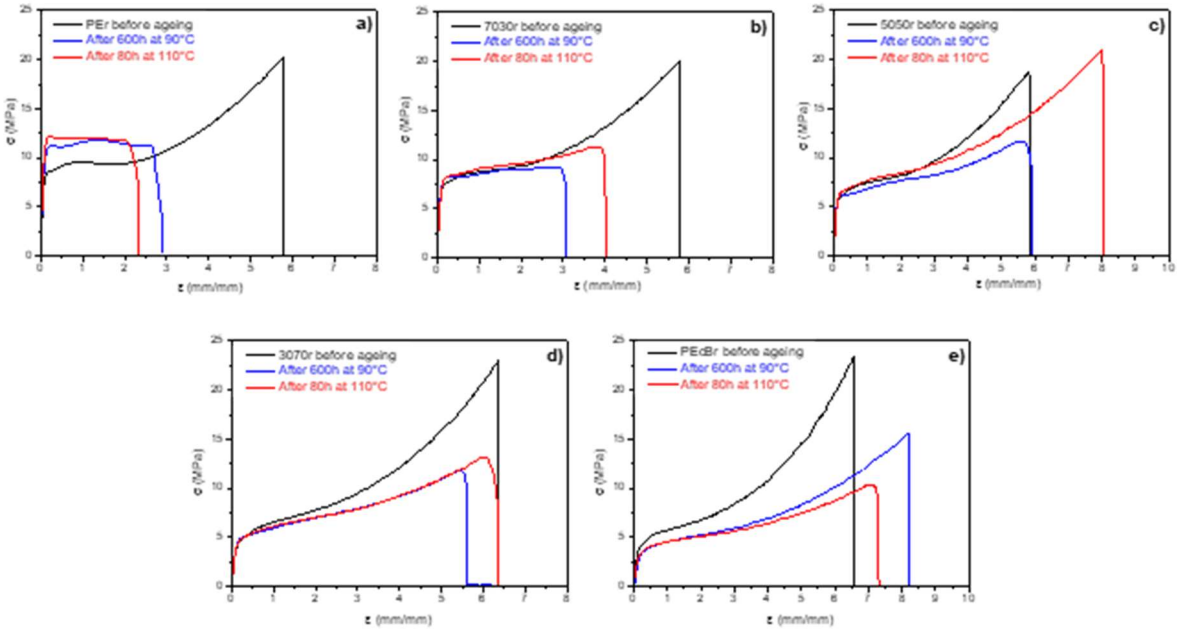

Fig. 13. Nominal stress-strain curves before and after thermal ageing at 90°C and 110°C for a) PEr b) 7030r c) 5050r d) 3070r and e) PEcBr.

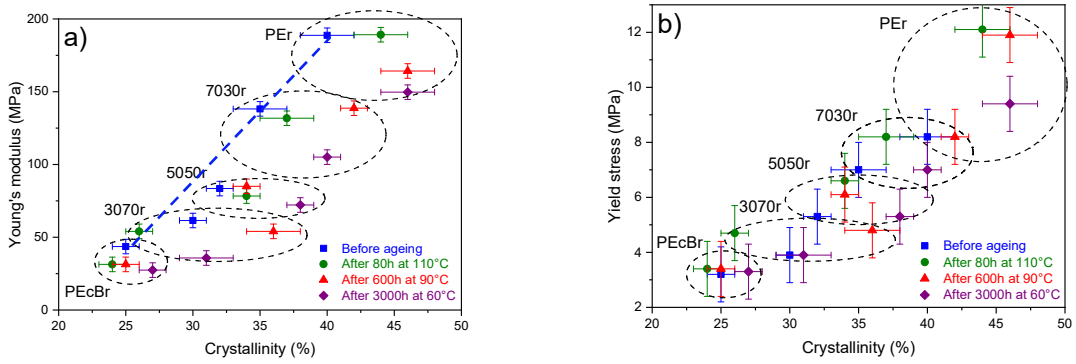

Fig. 14. Young's modulus (a) and yield stress plotted vs crystallinity for unaged samples and samples for 3000 h at 60°C, 600 h at 90°C and 80 h at 110°C.

The yield stress of the samples with the highest PEr content evolves as a function of the crystallinity, similar to the Young modulus, as shown in Figure 14b. More subtle differences may exist in relation to the semi-crystalline microstructure and the amorphous chain network. Nevertheless, the error made in their estimate is too large to provide further discussion. The strain hardening and rupture behaviour is also a complex result of the microstructure of the

materials. Regardless of the chosen ageing procedure, the slope of the stress-strain curve in its terminal part decreases. Only thermo-oxidized PEr (and to a lesser extent, 7030r) presents a peculiar behaviour, with no strain hardening (the sample breaks before its occurrence), and a higher yield stress than unaged PEr. This behaviour is related to the large increase in crystallinity promoted by ageing (for example, from 40 to 47% after 80 h of thermal ageing at 110°C). The rupture of the degraded materials is less sudden than in the non-degraded ones, especially for the highest PEr content. Again, note the peculiar behaviour of 5050r, which interestingly shows, when considering the global stress-strain curve, the best compromise in terms of resistance to ageing.

5. Conclusion

Our study confirms the importance of the butene content of crosslinked PE on its semi-crystalline microstructure. Changing the butene content from 3.4 wt% (for the so-called PE material) to 9.4 wt.% (PEcB) enlarges the distribution of the crystallite size and decreases the average size value and the total crystallinity. Moreover, the crystallites no longer organize themselves as large spherulites, even though the different size populations still seem to gather in separated domains (with a local crystallinity of approximately 30-35%). Actually, the microstructure of the PE/PEcB crosslinked blends can roughly be deduced from the microstructure of each PE via the volume fraction of each (indicating a kind of phase separation process at the scale of crystallites), even though there is a large fraction of cocrystals made of chains of both PEs.

The thermo-oxidative ageing of these systems mainly leads to chain scission. However, the induced modifications of these structures on the elastomer network architecture, the semi-crystalline microstructure, and, finally, the mechanical properties are complex.

A significant chemi-crystallization is observed for PEr during ageing, not for PEcB. This can be explained by the initially substantial crystallinity of the former, which slows the amorphous chain mobility and the crystallization kinetics of the unaged material. Thus, scission, which provides more freedom to the chains, eases their incorporation into the crystallite. In homopolymers, and in the blends, annealing also occurs. As expected, its magnitude is directly related to the volume fraction of crystallites whose melting temperature is just below the ageing temperature. Logically, during ageing, a combination of both effects, annealing and chemi-crystallization, occurs in the blend in relation to the fraction of both homopolymers. Moreover, the crystallized chains being protected from chain scission, the semi-crystalline microstructure

remaining at the ageing temperature has a direct effect on the way that the elastomer network (initially created by the crosslinking process) is modified. Thus, when the ageing temperature does not melt the large crystallites, these crystallites protect the long chain portions between chemical crosslinks. In addition, the larger the PE quantity is, the more that the spherulitic morphology is preserved, thereby promoting the percolation of the cut chains. Thus, the mechanical behaviour of the materials at ambient temperature or at temperatures above their melting temperature is the result of all these mechanisms. Moreover, it was found that the 5050r blend may be the best compromise in terms of mechanical properties and their preservation during thermo-oxidation.

We should conclude by emphasizing that our interpretation is based on a (necessarily) limited amount of experimental data regarding the microstructure of the studied materials, which it would therefore be useful to confirm with additional experiments. It is also founded on measurements of the crystallinity via a methodology, classically used but subject to errors, which would deserve to be confirmed by WAXS and via a different methodology for the treatment of the DSC data. Said differently, the first ambition of this article is to propose an interpretation grid whose relevance needs to be confirmed by future works.

.

Acknowledgements

The authors wish to thank the Materials Ageing Institute (MAI-SN) for financial support, Guillaume Gallot and Jean-François Larché (Nexans Research Center) for sample preparation and Olivier Boyron (C2P2 Lyon) for SEC measurements. We acknowledge SOLEIL for the provision of synchrotron radiation facilities, and we would like to thank Javier Perez for assistance in using the SWING beamline. Many thanks to Florent Dalmas for assistance in microscopy observations.

References

[1] H. Wen, H. Li, S. Xu, S. Xiao, H. Li, S. Jiang, L. An, Z. Wu, Shear effects on crystallization behavior of poly(ethylene-co-octene) copolymers, Journal of Polymer Research. 2012;19.

[2] S. Bensason, J. Minick, A. Moet, S. Chum, A. Hiltner, E. Baer, Classification of Homogeneous Ethylene-Octene copolymers based on comonomer contents, J Polym Sci: Part B: Polymer Physics. 1996; 34: 1301-1315.

[3] H.P. Wang, S.P. Chum, A. Hiltner, E. Baer, Comparing elastomeric behavior of block and random ethylene-octene copolymers, J Appl Polym Sci 2009; 113: 3236–3244.

[4] G. Rapp, J. Tireau, P.-O. Bussiere, J.-M. Chenal, L. Chazeau, J.-L. Gardette, S. Therias, Influence of the physical state of a polymer blend on thermal ageing, Polym Degrad Stab 2019; 163:161–173.

[5] H. Vogt, H. Enderle, U. Schulte, J. Hessel, Thermal ageing of PE 100 pipes for accelerated lifetime prediction under service conditions, Plastics Pipes XIV Budapest, Hungary (2008).

[6] J. Lacoste, D.J. Carlsson, Gamma-, Photo-, and Thermally-Initiated Oxidation of linear low Density Polyethylene: A Quantitative Comparison of Oxidation Products, Journal of Polymer Science: Part A: Polymer Chemistry. 1992; 30: 493-500.

[7] F. Khabbaz, A.C. Albertsson, S. Karlsson, Chemical and morphological changes of environmentally degradable polyethylene films exposed to thermo-oxidation, Polym Degrad Stab 1999; 63: 127-138.

[8] A.F. Reano, A. Guinault, E. Richaud, B. Fayolle, Polyethylene loss of ductility during oxidation: Effect of initial molar mass distribution, Polym Degrad Stab 2018; 14: 978-84.

[9] S.F. Chabira, M. Sebaa, C. G'sell, Oxidation and crosslinking processes during thermal aging of low-density polyethylene films, J Appl Polym Sci 2011; 5200-5208.

[10] R. Ferhoum, Analysis of Thermal Ageing Effect (Hold Time - Crystallinity Rate - Mechanical Property) on High Density Polyethylene (HDPE), International Journal of Materials Science and Applications 2013; 2: 109.

[11] B.M. Imane, A. Asma, C.S. Fouad, S. Mohamed, Weathering Effects on the Microstructure Morphology of Low Density Polyethylene, Procedia - Social and Behavioral Sciences. 2015; 195: 2228-2235.

[12] J.-I. Weon, Effects of thermal ageing on mechanical and thermal behaviors of linear low density polyethylene pipe, Polym Degrad Stab 2010; 95: 14-20.

[13] B. Fayolle, X. Colin, L. Audouin, J. Verdu, Mechanism of degradation induced embrittlement in polyethylene, Polym Degrad Stab 2007; 92: 231-238.

[14] B. Fayolle, E. Richaud, X. Colin, J. Verdu, Review: degradation-induced embrittlement in semi-crystalline polymers having their amorphous phase in rubbery state, J Mater Sci 2008; 43: 6999-7012.

[15] M.E. Acevedo, R. Quijada, M.C. Vallette, Thermal oxidation of metallocene ethylene-1-olefin copolymer films during one year oven aging, Polym Degrad Stab 2008; 93: 1947-1951.

[16] S. Al-Malaika, X. Peng, H. Watson, Metallocene ethylene-1-octene copolymers: Influence of comonomer content on thermo-mechanical, rheological, and thermo-oxidative behaviours before and after melt processing in an internal mixer, Polymer Degradation and Stab 2006; 91: 3131-3148.

[17] A. Perthué, P.-O. Bussière, M. Baba, J.-F. Larche, J.-L. Gardette, S. Therias, Correlation between water uptake and loss of the insulating properties of PE/ATH composites used in cables applications, Polym Degrad Stab 2016; 127: 79-87.

[18] M. Celina, G.A. George, Characterisation and degradation studies of peroxide and silane crosslinked polyethylene, Polym Degrad Stab 1995; 48: 297-312.

[19] L. Boukezzi, A. Boubakeur, C. Laurent, M. Lallouani, DSC Study of Artificial Thermal Aging of XLPE Insulation Cables, in: IEEE 2007; 146-149.

[20] J. Pospíšil, Z. Horák, Z. Kruliš, S. Nešpůrek, S. Kuroda, Degradation and aging of polymer blends I. Thermomechanical and thermal degradation, Polym Degrad Stab 1999; 65: 405-414.

[21] G. Singh, H. Bhunia, P.K. Bajpai, V. Choudhary, Thermal degradation and physical aging of linear low density polyethylene and poly(l-lactic acid) blends, J Polym Eng 2012; 32: 59-66.

[22] C. Sirisinha, P. Sae-Oui, J. Guaysomboon, Mechanical properties, oil resistance, and thermal aging properties in chlorinated polyethylene/natural rubber blends, J Appl Polym Sci 2002; 84: 22-28.

[23] S. Hassanpour, F. Khoylou, E. Jabbarzadeh, Thermal degradation of electron beam crosslinked polyethylene and (ethylene–vinylacetate) blends in hot water, J Appl Polym Sci 2003; 89: 2346-2352.

[24] R. Salehiyan, T. Malwela, S.S. Ray, Thermo-oxidative degradation study of melt-processed polyethylene and its blend with polyamide using time-resolved rheometry, Polym Degrad Stab 2017; 139: 130-137.

[25] W.L. Hawkins, W. Matreyek, and F. H. Winslow, The morphology of semicrystalline polymers. Part I. The effect of temperature on the oxidation of polyolefins, Journal of Polymer Science, 1959, 41.138: 1-11.

[26] F.H. Winslow, Recent studies of polymer degradation and stabilization. Die Makromolekulare Chemie: Macromolecular Chemistry and Physics, 1979, vol. 2, no S19791, p. 27-34.

[27] E.T. Hsieh, J.C. Randall, Ethylene-1-butene copolymers. 1. Comonomer sequence distribution, Macromolecules 1982; 15: 353-360.

[28] A. Nuamthanom, Multidimensional NMR Studies of Poly (ethylene-co-1-octene) Copolymers and Poly (ethylene-co-vinyl Acetate-co-carbon Monoxide) Terpolymers, PhD Thesis, University of Akron (2007).

[29] B. Wunderlich, Thermal Analysis, Academic Press 1990; 417-431.

[30] A.P. Gray, Polymer Crystallisation determination by DSC. Thermochemica Acta, 1970, 1: 563-579.

[31] C.G. Vonk, G. Kortleve, X-ray small-angle scattering of bulk polyethylene. Kolloid-Zeitschrift und Zeitschrift für Polymere, 1967, 220: 19-24.

[32] S. Bensason, J. Minick, A. Moet, A, S. Chum, A. Hiltner, E. Baer, Classification of Homogeneous Ethylene-Octene Copolymers Based on Comonomer Content. Journal of Polymer Science: Part B: Polymer Physics 1996, 34: 1301-15.

[33] S/W Lambert , P.J. Phillips Structural and melting studies of crosslinked linear polyethylenes. Polymer, 1990, vol. 31, 11:2077-2082.

[34] D. Montezinos, B. Gail Wells, J.L. Burns, The Use of Ruthenium in Hypochlorite as a Stain for Polymeric Materials, Journal of Polymer Science: Polymer Letters Edition. 1985; 23: 421-425.

[35] S. Schmitt, TEM analysis of microstructural morphology in ultra high molecular weight polyethylene, Scripta Materialia. 2000; 43: 523-528.

[36] F. Defoor, G. Groeninckx, P. Schouterden, B. Van der Heijden, Molecular, thermal and morphological characterization of narrowly branched fractions of 1-octene LLDPE: 2. Study of the lamellar morphology by transmission electron microscopy, Polymer 1992; 33: 5186-5190.

[37] R. Androsch, Melting and crystallization of poly (ethylene-co-octene) measured by modulated dsc and temperature-resolved X-ray diffraction, Polymer 1999; 40: 2805-2812.

[38] H. Wen, H. Li, S. Xu, S. Xiao, H. Li, S. Jiang, L. An, Z. Wu, Shear effects on crystallization behavior of poly(ethylene-co-octene) copolymers, Journal of Polymer Research 2012; 19: .

[39] A.G. Simanke, G.B. Galland, L. Freitas, J. Alziro H. da Jornada, R. Quijada, R.S. Mauler, Influence of the comonomer content on the thermal and dynamic mechanical properties of metallocene ethylene/1-octene copolymers, Polymer 1999; 40: 5489-5495.

[40] H.P. Wang, S.P. Chum, A. Hiltner, E. Baer, Comparing elastomeric behavior of block and random ethylene-octene copolymers, J Appl Polym Sci 2009; 113: 3236–3244.

[41] S.V. Eynde, V.B.F. Mathot, M.H.J. Koch, H. Reynaers, Thermal behaviour and morphology of homogeneous ethylene–1-octene copolymers with high comonomer contents, Polymer 2000; 41: 4889-4900.

[42] M. Zhang, D.T. Lynch, S.E. Wanke, Effect of molecular structure distribution on melting and crystallization behavior of 1-butene/ethylene copolymers, Polymer 2001; 42: 3067-3075.

[43] S.V. Eynde, V. Mathot, M.H.J. Koch, H. Reynaers, Thermal behaviour and morphology of homogeneous ethylene–propylene and ethylene–1-butene copolymers with high comonomer contents, Polymer 2000; 41: 3437-3453.

[44] J. Xu, X. Xu, L. Chen, L. Feng, W. Chen, Effect of composition distribution on miscibility and co-crystallization phenomena in the blends of low density polyethylene with conventional and metallocene-based ethylene±butene copolymers, Polymer 2001; 42: 3867-3874.

[45] C.A. Fonseca, I.R. Harrison, An investigation of co-crystallization in LDPE/HDPE blends using DSC and TREF, Thermochimica Acta 1998; 313: 37-41.

[46] R.L. Morgan, M.J. Hill, P.J. Barham, Morphology, melting behaviour and co-crystallization in polyethylene blends: the effect of cooling rate on two homogeneously mixed blends, Polymer 1999; 40: 337-348.

[47] C. Frederix, J.M. Lefebvre, C. Rochas, R. Séguéla, G. Stoclet, Binary blends of linear ethylene copolymers over a wide crystallinity range: Rheology, crystallization, melting and structure properties, Polymer 2010; 51: 2903-2917.

[48] C. Ślusarczyk, Time-resolved SAXS studies of morphological changes in a blend of linear polyethylene with homogeneous ethylene-1-octene copolymer, Nuclear Instruments and Methods in Physics Research Section B: Beam Interactions with Materials and Atoms. 2015; 364: 116-119.

[49] R. Androsch, J. Blackwell, S.N. Chvalun, B. Wunderlich, Wide- and Small-Angle X-ray Analysis of Poly(ethylene-co-octene), Macromolecules 1999; 32: 3735-3740.

[50] V.B.F. Mathot, R.L. Scherrenberg, M.F.J. Pijpers, W. Bras, Dynamic DSC, SAXS and WAXS on homogeneous ethylene-propylene and ethylene-octene copolymers with high comonomer contents, J Therm Anal 1996; 46: 681-718.

[51] B. Xiong, O. Lame, J.-M. Chenal, C. Rochas, R. Seguela, G. Vigier, In-situ SAXS study of the mesoscale deformation of polyethylene in the pre-yield strain domain: Influence of microstructure and temperature, Polymer 2014; 55: 1223-1227.

[52] Q. Fu, Y. Men, G. Strobl, Understanding of the tensile deformation in HDPE/LDPE blends based on their crystal structure and phase morphology, Polymer 2003; 44: 1927-1933.

[53] B. Xiong, O. Lame, R. Seguela, Y. Men, Micro/macro-stress relationship and local stress distribution in polyethylene spherulites upon uniaxial stretching in the small strain domain, Polymer 2018; 140: 215-224.

[54] S. Humbert, O. Lame, G. Vigier, Polyethylene yielding behaviour: What is behind the correlation between yield stress and crystallinity?, Polymer 2009; 50: 3755-3761.

[55] D. Rana, C.H. Lee, K. Cho, B.H. Lee, S. Choe, Thermal and Mechanical Properties for Binary Blends of Metallocene Polyethylene with Conventional Polyolefins, J Appl Polym Sci 1998; 69: 2441-2450.

[56] S. Humbert, O. Lame, R. Séguéla, G. Vigier, A re-examination of the elastic modulus dependence on crystallinity in semi-crystalline polymers, Polymer 2011; 52: 4899-4909.

[57] C. Li Pi Shan, J.B.P. Soares, A. Penlidis, Mechanical properties of ethylene/1-hexene copolymers with tailored short chain branching distributions, Polymer 2002; 43: 767-773.

[58] K. Jordens, G.L. Wilkes, J. Janzen, D.C. Rohlfing, M.B. Welch, The influence of molecular weight and thermal history on the thermal, rheological, and mechanical properties of metallocene-catalyzed linear polyethylenes, Polymer 2000; 41: 7175-7192.

[59] K.E. Figueroa, Thermoanalytical study of an aged XLPE-pipe, Thermochimica Acta 1987;114: 115-124.